Design of four-element MIMO antenna system for intelligent internet of everything (IIoE)

Aziz DKIOUAK (dkiouakaziz@hotmail.fr)
Abdelmalek Essaadi University
Mohssine EL OUAHABI
Abdelmalek Essaadi University
Alia ZAKRITI
Abdelmalek Essaadi University
Saad CHAKKOR
University of Abdelmalek Essaâdi
Mostafa BAGHOURI
University of Hassan II

Research Article

Keywords: MIMO antenna, IIoE, 5G, millimeter wave, orthogonal polarization

Posted Date: August 3rd, 2022

DOI: https://doi.org/10.21203/rs.3.rs-1903286/v1

Design of four-element MIMO antenna system for intelligent internet of everything (IIoE)

Aziz DKIOUAK [a], Mohssine EL OUAHABI [a], Alia ZAKRITI [a], Saad CHAKKOR[b] and Mostafa BAGHOURI [c]

[a] Abdelmalek Essaadi University, National School of applied Sciences, Tetuan, Morocco
dkiouakaziz@hotmail.fr

[b] LabTIC, ENSA of Tangier, University of Abdelmalek Essaâdi, Tangier, Morocco

[c] Systems Team, Structural Engineering, Intelligent Systems and Electrical Energy Laboratory, ENSAM of Casablanca, University of Hassan II, Morocco

Abstract:

In this paper, the design of four-element Multiple Input Multiple Output (MIMO) antenna systems has been proposed for intelligent internet of Everything (IIoE) and high-speed data applications. The presented antenna design operates at 4.9 GHz (5G millimeter wave applications) with high isolation in a small size. Defected Microstrip Structure (DMS), slot modification and orthogonal polarization are used to create the desired frequency band, improve the impedance bandwidth and enhance the isolation between the antenna elements at 4.9 GHz, respectively. Furthermore, the usefulness of the proposed MIMO antenna has been verified by comparing the simulated and the measured results using a fabricated version of the considered 4x4 MIMO antenna. In addition, the results indicate a high diversity performance in terms of: Envelope Correlation Coefficient (ECC), Diversity Gain (DG), Total Active Reflection Coefficient (TARC) and Total Channel Capacity Loss (CCL_{Total}).

Key words: MIMO antenna, IIoE, 5G, millimeter wave, orthogonal polarization.

1. INTRODUCTION

Among the greatest things about our time is that 5G is contributing to the realization of the Intelligent Internet of Everything, making big changes in people's lives and in many verticals industries, making the world a better connected and digital one [1]. A key feature of 5G is the use of MIMO antenna arrays to meet the high

performance and new service requirements of this amazing new era. The use of this kind of antenna in a network offers an unprecedented variety of possibilities. This includes increasing the channel capacity and data rates of individual links between the base station and mobile users, and reducing interference between individual users and cells [2]. To realize the MIMO operation for 5G smartphones, the multi-antenna design can be used to provide polarization and pattern diversity for reliable communication with minimum mutual coupling [3-4]. A lot of research efforts have been put to increase the number of antenna elements in a limited space to improve the overall system capacity and bandwidth utilization [5]. However, the placement of multiple antenna elements on the receiving terminal in a small space causes significant problems such as low isolation between the antenna elements [6]. Therefore, several recent techniques have been applied to minimize the mutual coupling amid closely spaced antennas. In refs. [7-11], they include defected ground structures (DGS) to improve the antenna radiation performance, to allow efficient coupling with the feed line and also to alter the shield current distribution in the ground according to the shape and size of the defect. A Compact MIMO antenna with Electromagnetic Band gap (EBG) structure for isolation enhancement has been presented in ref. [12]. The Transmission Line Decoupling Network (TLDN) technique is presented in ref. [13] to enhance the isolation of a dual-band multiple input and multiple output (MIMO) antenna. In ref. [14], a Neutralization Line Decoupling (NLD) is inserted between the elements to realize decoupling. El Ouahabi et al. [15] have conceived a miniaturized dual-band MIMO antenna with low mutual coupling for wireless applications. It is designed using orthogonal microstrip feed line and a Single Complementary Split Ring Resonator (S-CSRR) to improve their performance. Another approach using orthogonal polarization was the main idea for the design of a MIMO antenna with low mutual coupling has been published in refs. [16-17]. The combination of orthogonal polarization and DGS structure is another solution to improve the performance of the MIMO antenna.

In this paper, a novel 4-port MIMO antenna array that can cover 200 MHz (4.08%) at 4.9 GHz for future 5G applications has been designed. The four antenna elements are symmetrically patterned on FR-4 substrate in a compact size of 29 × 50 ×1.6 mm^3 ($0.47\lambda_0 \times 0.81\lambda_0 \times 0.02\lambda_0$, where λ_0 = guided wavelength at the lowest operating frequency). The combination of three different methods (DMS, slot modification and orthogonal polarization) is used to improve the performance of the proposed MIMO antenna. Due to it has: High isolation between the 4-ports element antenna, good impedance matching, small size, a simple structure and is easy in fabrication. It has an excellent model for use in 5th generation portable devices.

2. ANTENNA DESIGN

2.1.Antenna Geometry

The model of 2x2 MIMO antenna is etched on FR-4 substrate with a dielectric constant ε_r = 4.4, a loss tangent δ=0.02 and a thickness of 1.6 mm (figure 1). The two symmetrical F-shaped antenna elements printed on the top face of the substrate and each of them is fed by a 50 Ω microstrip line. On the other side, two symmetrical slots of 0.5 mm width etched on the bottom to improve the impedance matching at 4.9 GHz.

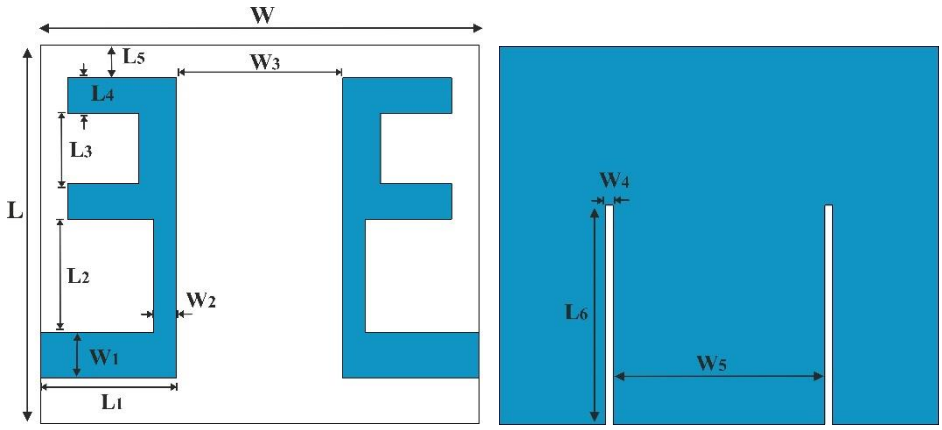

(a) (b)

Figure 1. Configuration of the proposed MIMO antenna: (a) Front view, (b) Bottom view.

2.2.Antenna Design Process

Figure 2, displays the different phases of the design process of the proposed antenna. It steps from Ant. i, through Ant. ii to Ant. iii. In conjunction with this, figure 3 represents the corresponding results of the simulated S-parameters at each step. During the design process, the Microwave Studio software from Computer Simulation Technology (CST) is employed to implement the simulation and optimization of the antenna. The description of the different design steps of this new MIMO antenna is presented in the following.

The first step of the proposed MIMO antenna begins with two rectangular patches that are symmetrically etched side by side on the top face of the FR4 substrate with a full backed ground. Each antenna is powered by a 50 ohm microstrip line to provide a connection between the antenna and the external source via an SMA connector. The two feeding lines are initially parallel to each other (Ant. i) in figure 2. In order to create the resonant frequency at 4.9 GHz for 5G millimeter wave applications and to increase the effective surface current path length, an area of 21.85 mm^2 is charged on the rectangular patches (Ant. ii). According to the simulation results, the -10 dB bandwidth is able to cover the desired frequency band (4.9 GHz) with a span of 4.73 to 5.02

GHz. Furthermore, the simulated isolation between the antenna elements is equal to -20.5 dB. In the final design, we are changing the parallel feeding method to the orthogonal microstrip feed line to enhance the isolation between the two ports (Ant. iii) in figure 2. In addition, we have etched a slot on the bottom layer under each antenna to obtain a better matching of the resonant frequency band. As can be seen in figure 3, the corresponding results of Ant. iii show a monoband antenna element of 200 MHz bandwidth (4.80–5.00 GHz), with a mutual coupling of less than −20 dB.

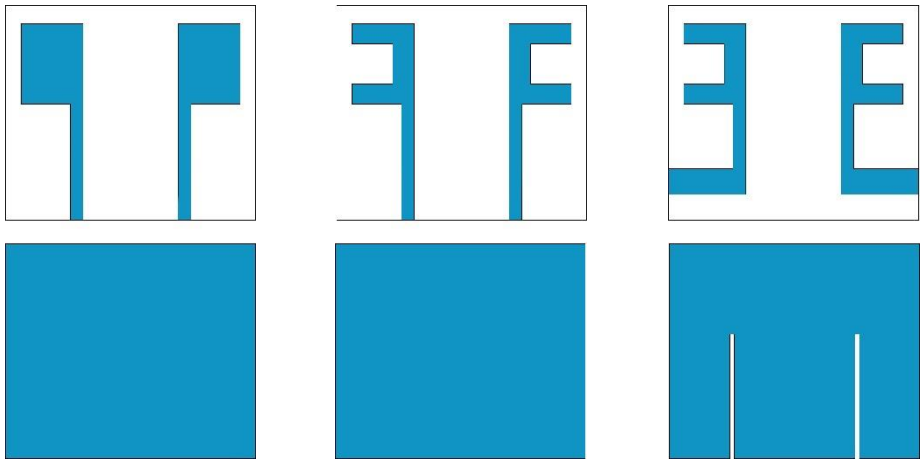

Ant. i Ant. ii Ant. iii

Figure 2. Design evolution of the compact MIMO antenna

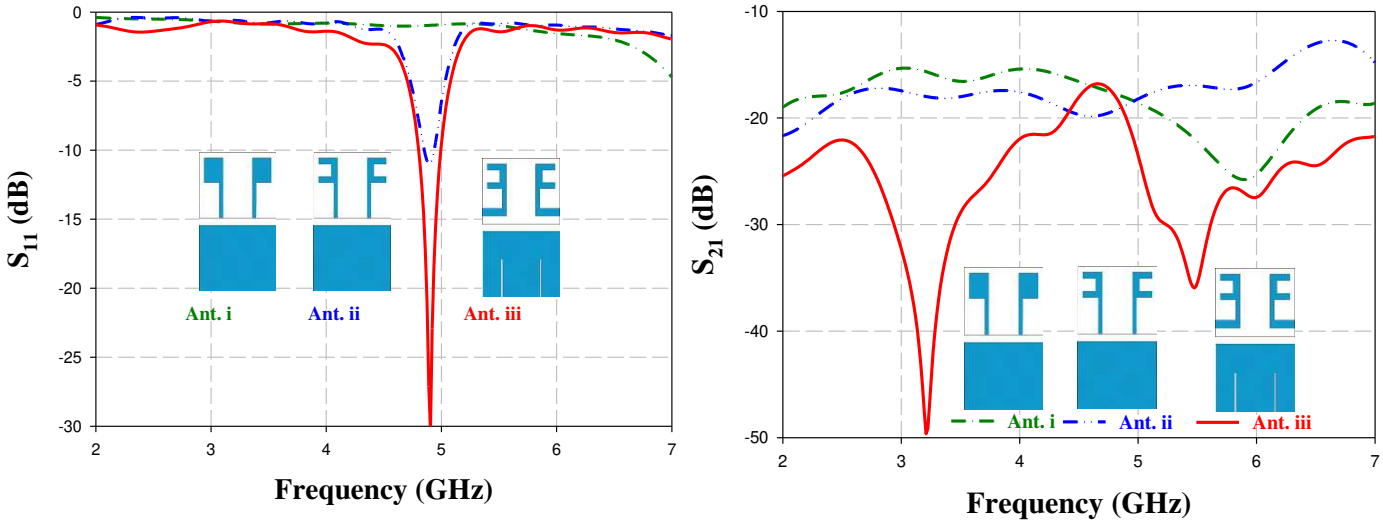

(a) (b)

Figure 3. S-parameters of three different antennas: (a) S_{11}, (b) S_{21}

2.3.Four-Element Mimo Antenna

Increasing the number of MIMO antennas at the transmitters and receivers can improve the communication quality and increase the channel capacity without additional radiation power and spectrum bandwidth. For this purpose, we have doubled the number of transmitters and receivers from two to four antennas, as shown in the following figure. The overall size of the proposed structure is 50 × 29 mm^2. As illustrated in figure 4, the compact design of a 4-element MIMO antenna is proposed, which are indicated by P_1, P_2, P_3, and P_4.

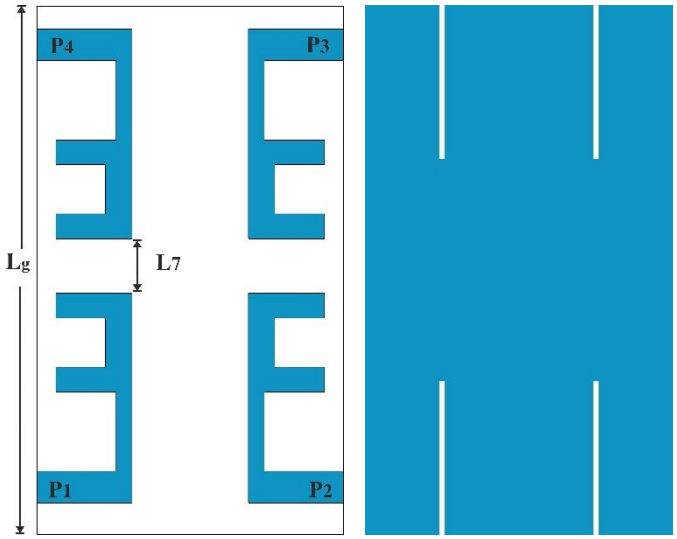

Figure 4. Four-element MIMO antenna system

The complete structure with its dimensions is shown in figure 1 and figure 4. The displayed MIMO antenna is conceived and simulated through the CST software. The values of this structure are reported below in table 1.

Table 1: Optimized antenna parameters

Parameters	W	L	L_g	W_1	W_2	W_3	W_4	W_5	L_1	L_2	L_3	L_4	L_5	L_6	L_7
Values (mm)	29	24	50	3	1.5	11	0.5	14	9	7.5	4.65	2.35	0.74	14.5	5.15

The simulated S parameters of the proposed antenna are shown in figure 5. Due to the symmetry, the analysis of the S-parameters can be easily carried out by considering $S_{11} = S_{22} = S_{33} = S_{44}$, $S_{21} = S_{12} = S_{34} = S_{43}$, $S_{13} = S_{31} = S_{42} = S_{24}$, and $S_{14} = S_{41} = S_{23} = S_{32}$. According to this figure, the scattering parameters of the 4-element MIMO antenna system are adapted to the desired frequency band with -34 dB. On the same plot, the frequency bandwidth of less than −10 dB is 4.08% (4.8 to 5.0 GHz), which is appropriate for the reflection coefficient requirement for 5G applications. Furthermore, it shows that a minimum isolation level ~~higher~~ of more than -20

dB is achieved over the entire frequency band between the four ports, which proves the good performance of the proposed four-element MIMO antenna.

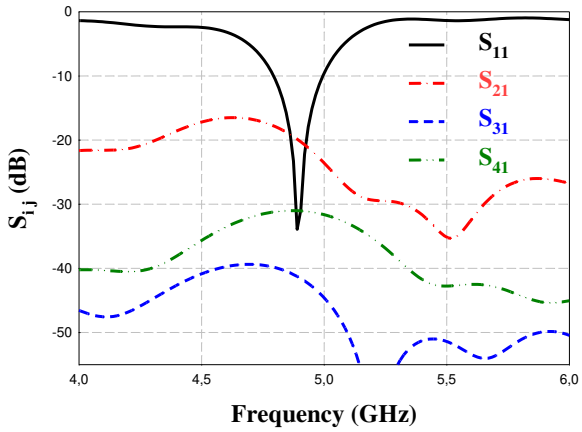

Figure 5. The simulated S parameters of the proposed four-element MIMO antenna

3. ANTENNA PERFORMANCE

3.1.Fabrication and Measurement

The fabricated prototype of the presented MIMO antenna is shown in figure 6. The fabrication process is carried out in the laboratories of Abdelmalek Essaâdi University. It is done using a printed circuit board (PCB) milling machine: The LPKF Protomat E33. The Rohde and Schwarz ZVB 20 vector network analyzer is used to measure its performance. For the given MIMO antenna system, when antenna i-port is excited, the other ports were terminated with 50 Ω.

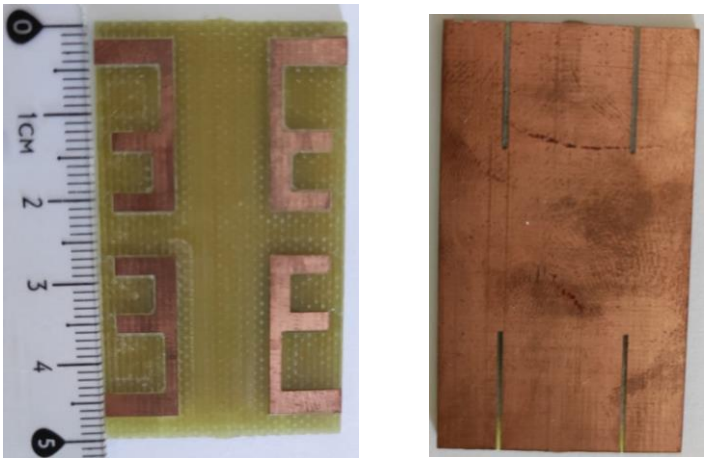

(a) (b)

Figure 6. Photograph of the fabricated MIMO antenna. (a) Top side. (b) Back side.

The measured reflection coefficient for all the four antenna elements is identical due to the physical symmetry; hence, only one of the four results is shown. The measured −10 dB impedance bandwidth is 430 MHz (4.68GHz–5.11 GHz) with -22 dB at the desired frequency band and covers a 5G millimeter wave application.

In order to check how tightly coupled the antenna elements are, measured isolation curves are presented in the figure 7 (b). All the four antenna elements are placed symmetrically on the PCB board. Only S_{12}, S_{13} and S_{14} curves are given. The minimum isolation was observed between the ports (P_1 and P_2) and equal -22dB. Other ports (P_1 and P_3 ; P_1 and P_4) are separated by large distance and isolation values observed are better than -28 dB at the operation band (4.9 GHz).

As shown in figure 7, a good agreement between the simulated and measured curves is evident. Moreover, the deviation between the both results is due to the fabrication errors, parasitic effects and SMA connector losses.

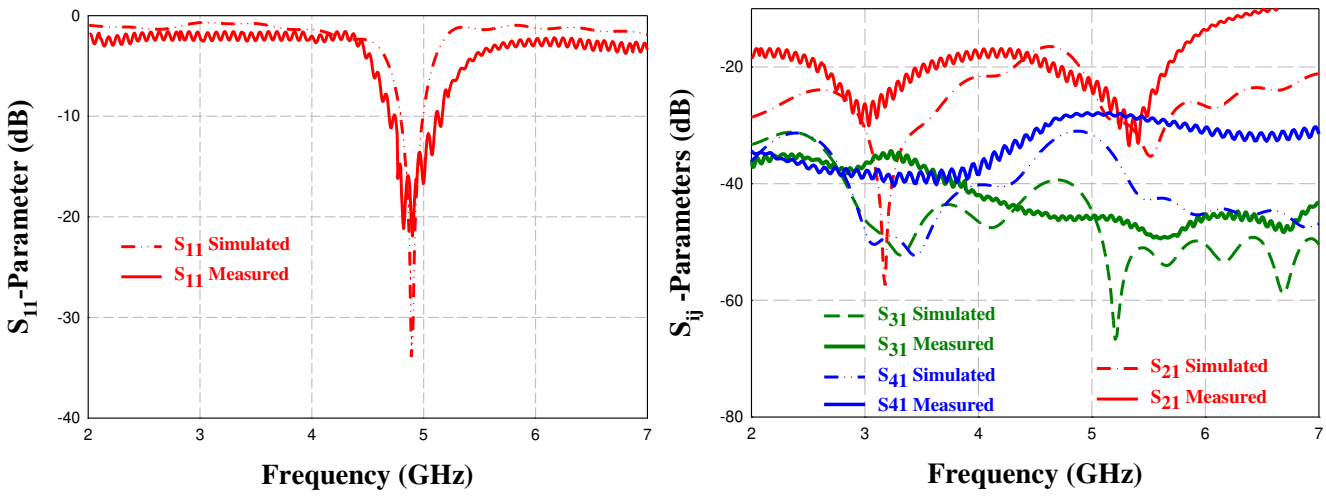

(a) (b)

Figure 7. Measured and simulated of the fabricated four-element MIMO antenna. (a) S_{11}. (b) S_{21}, S_{31} and S_{41}.

3.2.Envelope Correlation Coefficient and Diversity Gain

The envelope correlation coefficient depicts the correlation between radiating elements and how much their radiation patterns affect each other when they are operating at the same time. This coefficient must be lower than 0.5 to obtain a good diversity gain.

For the i^{th} and j^{th} antenna elements, the calculation of this coefficient using the far-field patterns [18-19] can be done from (1):

$$ECC(i,j)=\frac{\left|\oint\left(X_{PR}E_{\theta i}(\Omega)E^{*}_{\theta j}(\Omega)P_{\theta}(\Omega)+E_{\varphi i}(\Omega)E^{*}_{\varphi j}(\Omega)P_{\varphi}(\Omega)\right)d(\Omega)\right|^{2}}{\oint\left(X_{PR}G_{\theta i}(\Omega)P_{\theta}(\Omega)+G_{\varphi i}(\Omega)P_{\varphi}(\Omega)\right)d(\Omega).\oint\left(X_{PR}G_{\theta j}(\Omega)P_{\theta}(\Omega)+G_{\varphi j}(\Omega)P_{\varphi}(\Omega)\right)d(\Omega)} \quad (1)$$

Where, X_{PR} denotes cross-polarization power ratio of the propagation environment. In the formula above, $G_{\theta}(\Omega)=E_{\theta}(\Omega)E^{*}{}_{\theta}(\Omega)$ and $G_{\varphi}(\Omega)=E_{\varphi}(\Omega)E^{*}{}_{\varphi}(\Omega)$ are the power patterns of θ and φ polarizations, respectively. $P_{\theta}(\Omega)$ and $P_{\varphi}(\Omega)$ denote the angular density functions of the θ and ϕ polarizations, respectively.

$E_{\theta i}(\Omega)$ and $E_{\theta j}(\Omega)$ are the electric field patterns of the ith and jth antenna elements in the θ polarization, respectively. $E_{\varphi i}(\Omega)$ and $E_{\varphi j}(\Omega)$ are the electric field patterns of the ith and jth antenna elements in the φ polarization, respectively.

In the case of a (4, 4) MIMO system, with N=4 antennas at both ends, the ECC between antenna i=1 and j=2, 3, 4 are shown in figure 8 (a).

In case of the lossless antenna, the ECC is calculated from the S parameters [20] by using the equation (2):

$$ECC=\frac{\left|\sum_{n=1}^{N}S^{*}_{i,n}S_{n,j}\right|^{2}}{\prod_{k=i,j}\left[1-\left|\sum_{n=1}^{N}S^{*}_{i,n}S_{n,k}\right|\right]} \quad (2)$$

The diversity gain can be calculated from the ECC by the below approximate formula [18-19].

$$DG=10\sqrt{\left(1-|\rho|^{2}\right)} \quad (3)$$

Where ρ is the complex cross correlation coefficient, and $|\rho|^{2}=ECC$

Figures 8 and 9 represents the ECC and DG curves simulated from the radiation patterns (3D) and S-parameters.

Where ECC(1,2), ECC(1,3) and ECC(1,4) are envelope correlations between the antennas 1, 2, antennas 1, 3 and antennas 1, 4 (antennas numbers are indicated in figure 4), respectively.

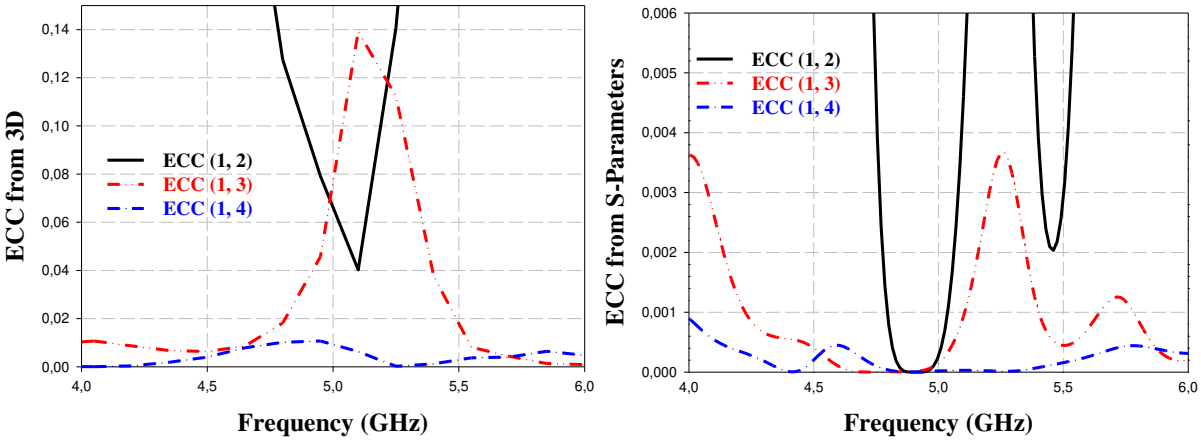

(a) (b)

Figure 8: ECC curve: (a) from 3D and (b) from S parameters

The ECC value extracted from 3D is less than 0.08 as shown in figure 8 (a) and very low (near to zero) in the case of lossless antenna (figure 8 (b)). These two values are within the permissible limit, which illustrates a very good diversity performance. On the other hand, the MIMO antenna yields a diversity gain greater than 9.8 at 4.9 GHz as shown in figure 9.

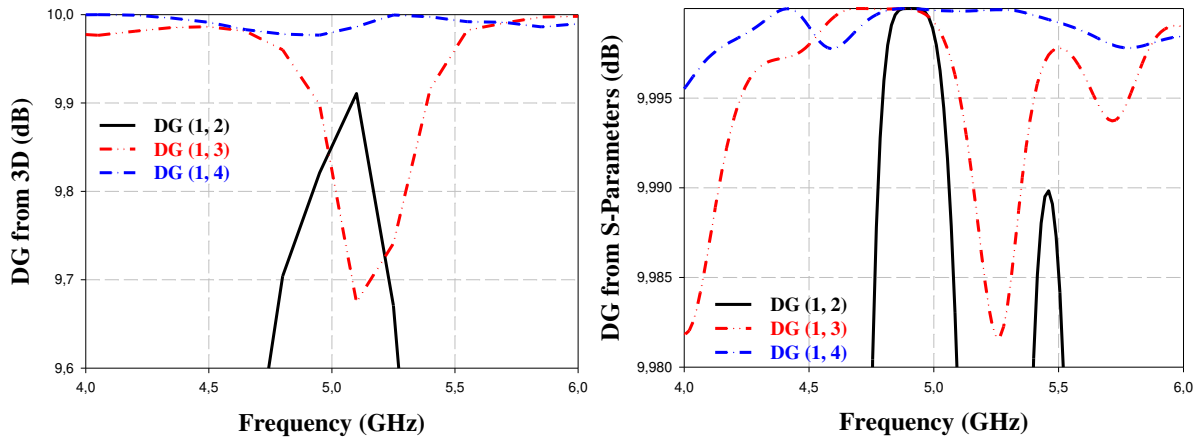

(a) (b)

Figure 9: DG curve: (a) from 3D and (b) from S parameters

3.3.Total Active Reflection Coefficient and Total Channel Capacity Loss

The specific parameter to more accurately describe the bandwidth and efficiency of the MIMO system is the TARC. The value of this parameter signifies how much power is radiated from the MIMO antenna ~~concerning~~ relative to the incident power at a particular phase angle. The TARC can be determined using the S-parameters [21-22]. In the case of a four ports MIMO antenna, the TARC is defined as follows:

$$\mathrm{TARC} = \sqrt{\frac{|S_1|^2+|S_2|^2+|S_3|^2+|S_4|^2}{2}} \quad (4)$$

Where:

$$S_1 = \mathrm{S}_{11} + \mathrm{S}_{12}\mathrm{e}^{\mathrm{j}\theta} + \mathrm{S}_{13}\mathrm{e}^{\mathrm{j}\theta'} + \mathrm{S}_{14}\mathrm{e}^{\mathrm{j}\theta''}$$

$$S_2 = \mathrm{S}_{21} + \mathrm{S}_{22}\mathrm{e}^{\mathrm{j}\theta} + \mathrm{S}_{23}\mathrm{e}^{\mathrm{j}\theta'} + \mathrm{S}_{24}\mathrm{e}^{\mathrm{j}\theta''}$$

$$S_3 = \mathrm{S}_{31} + \mathrm{S}_{32}\mathrm{e}^{\mathrm{j}\theta} + \mathrm{S}_{33}\mathrm{e}^{\mathrm{j}\theta'} + \mathrm{S}_{34}\mathrm{e}^{\mathrm{j}\theta''}$$

$$S_4 = \mathrm{S}_{41} + \mathrm{S}_{42}\mathrm{e}^{\mathrm{j}\theta} + \mathrm{S}_{43}\mathrm{e}^{\mathrm{j}\theta'} + \mathrm{S}_{44}\mathrm{e}^{\mathrm{j}\theta''}$$

With θ, θ' and θ'' are the phase differences between the excitation ports.

Therefore, TARC contains the effect of mutual coupling and feed phases and can be defined as the return loss coefficient of the entire MIMO antenna array [23]. Once the S-parameters of the antenna ports have been found, the random phases are swept between 0 and 180 degrees to study the effect of the phase variation between the ports, thus creating the corresponding TARC curves [23].

From the figure 10, the TARC value is well below than −15 dB at 4.9 GHz which meets the criteria for MIMO performance.

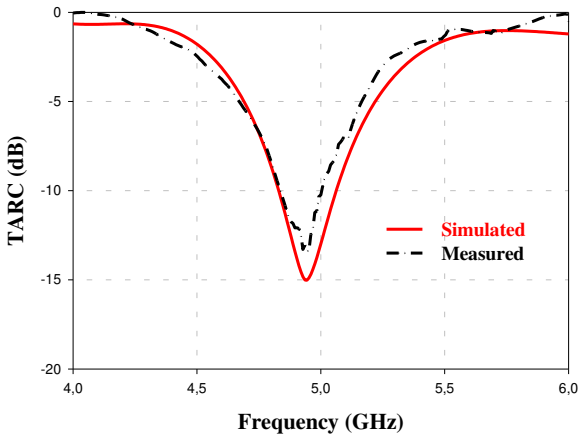

Figure 10: The simulated and the measured TARC of the presented MIMO antenna

The CCL has been enlisted among the MIMO performance parameters, thus providing details on the capacity losses of the system channels during the correlation effect. Ideally, the CCL value should be less than 0.4

bits/Hz in all operating bands [24]. In addition, the capacity of the MIMO system grows as the number of antennas increases. Mathematically, the CCL can be defined by equation (5) [25].

$$CCL = -log_2 det(\psi^R) \tag{5}$$

Where ψ^R Represents the correlation matrix of the receiving antennas is given mathematically as:

$$\psi^R = \begin{bmatrix} \rho_{11} & \rho_{12} & \rho_{13} & \rho_{14} \\ \rho_{21} & \rho_{22} & \rho_{23} & \rho_{24} \\ \rho_{31} & \rho_{32} & \rho_{33} & \rho_{34} \\ \rho_{41} & \rho_{42} & \rho_{43} & \rho_{44} \end{bmatrix} \tag{6}$$

Where: $\rho_{ii} = 1 - |\sum_{n=1}^{M} S_{in}^* \times S_{ni}|$ and $\rho_{ij} = -\sum_{n=1}^{M} S_{in}^* \times S_{nj}$ for $i, j = 1, 2, 3\ and\ 4$

ρ_{ii} et ρ_{ij} are the correlation coefficients

For more realistic results, the transmission power losses due to the TARC coefficient are also considered. Therefore, the global capacity loss of the channel [26] is in the following form:

$$CCL_{Total} = -2log_2(1 - TARC^2) - log_2 det(\psi^R) \tag{7}$$

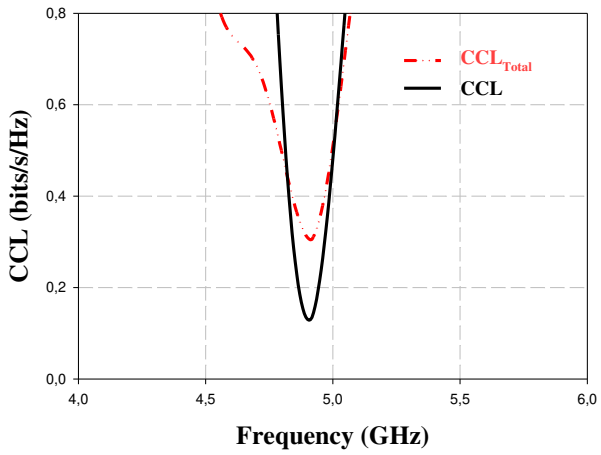

Figure 11: CCL and CCL_{Total} curve of the MIMO antenna

3.4.MIMO Channel Capacity

In this section, we study the MIMO channel capacity of our MIMO antenna over the SNR range from 0 to 20 dB. The theoretical capacity of this system, with MT transmitting and NR receiving antennas, is defined by the following formula [27-28]:

$$C_{MIMO} = \log_2\left(\det\left[I_{Nt} + \frac{\gamma}{Mr} HH^H\right]\right) \quad \text{bit/s/Hz} \tag{8}$$

Where I_{Nt} is the identity matrix of dimension Nt × Mr.

The variable H is the channel matrix. The parameter H^H is the Hermitian transform of the H matrix defined by the transposed complex conjugate.

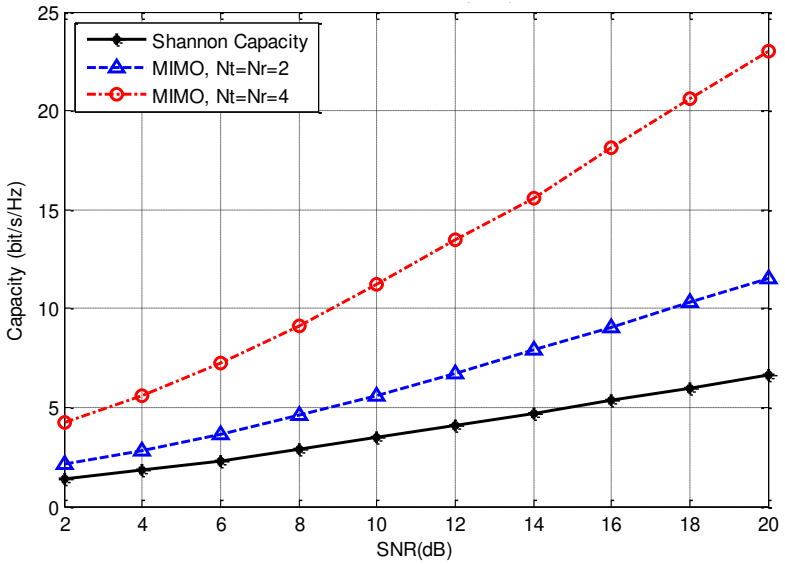

Figure 12 : MIMO capacity compared to SISO

The comparative study established in our case concerns the Shannon capacity with two MIMO 2x2 and 4x4 systems, each having the same number of antennas (Nt=Nr) on both the transmitter and receiver sides as shown in figure 12. The results obtained by the Matlab simulator show, for the three cases considered, a clear increase in the average capacity as a function of SNR, this increase, in favor of the MIMO 4x4 system, is all the more remarkable for high SNR values. According to this figure, the channel capacity at 20 dB SNR for 2x2 MIMO is about 12 bit/s/Hz and for 4x4 MIMO is about 23 bit/s/Hz, a significant difference of about 11 bit/s/Hz. In general, as the number of antennas increases, the average capacity increases.

3.5.Radiation Pattern

The normalized 2D far-field patterns simulated and measured the E-plane and H-plane for the suggested MIMO antenna at 4.9 GHz are shown in figure 13. Due to the symmetry, the radiation patterns of a single antenna element have been analyzed when the other elements are connected to a 50 ohm matching load.

According to this figure, the radiation patterns in the H-plane are also Omni-directional (takes the form of 'O') to receive signals equally from any direction, whereas in the E-plane it is quasi-omnidirectional (nearly omnidirectional) instead of being dipole-like. This is due to the current flowing on the protuberant ground plane, which leads to the zero being away from the E-plane. Note that because of measurements constraints and

lack of anechoic chamber, a slight difference between simulated and measured patterns has been observed. Due to the absence of an anechoic chamber, the measurements of the radiation patterns were not carried out inside an anechoic chamber, but in a free space. So, the measured result is slightly distorted compared with the simulated one.

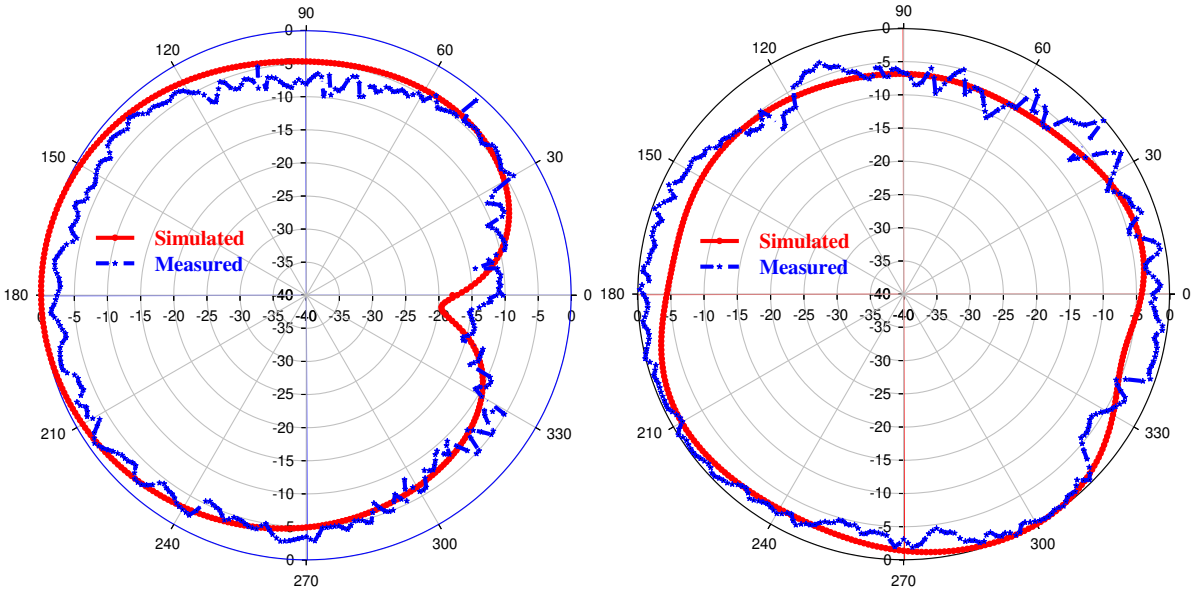

(a) (b)

Figure 13: Measured and simulated far-field pattern for E and H planes at 4.9 GHz: (a) E-plane and (b) H-plane.

4. PERFORMANCE COMPARAISON

Table 2 summarizes the comparison of the proposed four-element MIMO antenna array with previously reported MIMO antennas. This comparison has been made according to several parameters that characterize it. It is observed that the proposed MIMO antenna occupies a smaller area with high performance at 4.9 GHz in terms of isolation ECC (<0.08), DG (>9.8), TARC (<-10), and CCL (<0.4 b/s/Hz) compared to the previously reported work in this context [19, 25, 29, 31 and 32]. The suggested four-element MIMO antenna system has a very simple structure, high isolation achieved by using orthogonal polarization and a low cost FR-4 substrate compared to the reported works.

Table 2. Performance Comparison between our structure and other reported MIMO antenna

Ref. N°	Size in term of (mm^2 and λ_0)	Isolation (dB)	Isolation technique	ECC	CCL (bits/Hz)	TARC (dB)	Sub.
P.S	29×50=1450 $0.47\lambda_0 \times 0.81\lambda_0$	-20	Orthogonal polarization	< 0.08	<0.4	<-10	FR-4
[19]	40×40=1600 $1\lambda_0 \times 1\lambda_0$	-26	U-slot DGS	<0.02	-	-	FR-4
[25]	37×46=1702 $0.31\lambda_0 \times 0.38\lambda_0$		Orthogonal	<0.005	0.3	-	FR-4
[29]	67×138=9246 $0.8\lambda_0 \times 1.66\lambda_0$	-15	Orthogonal adjustment	<0.005	<0.19	-	Rogers 5880
[31]	40×40=1600 $0.32\lambda_0 \times 0.32\lambda_0$	-14	Orthogonal adjustment	<0.1	-	-	FR-4
[32]	110×110=12100 $0.62\lambda_0 \times 0.62\lambda_0$	-20	Orthogonal / Slots	<0.0025	-	<-10	FR-4

P.S= proposed structure and sub=substrate

5. CONCLUSION

In this paper, a 4-port antenna array for intelligent internet of everything and high speed data applications is proposed and investigated. DMS, slot modification and orthogonal polarization are three different techniques that were used to design the proposed antenna with high performance. In spite of a very compact area, the proposed antenna exhibits high inter-element isolation (Sij≥ −20 dB) and good impedance matching (Sii≥−10 dB) at 4.9 GHz. The findings show that the ECC, DG, TARC, CCL_{Total} and MIMO channel capacity are excellent results for MIMO applications over the proposed band.

6. ACKNOWLEDGMENT

This work was partially supported by the faculty of sciences, under information systems and telecommunications laboratory, Abdelmalek Essaadi University, Tetuan, Morocco, Supervised by Professor Mohsine Khalladi.

The authors would like to thank Professor Naima Amar Touhami of Abdelmalek Essaâdi University, Tetuan, Morocco, for providing the measurements facilities.

COMPETING INTERESTS

The authors have not disclosed any competing interests.

REFERENCES

[1] N. Application, “5G Massive MIMO Network Application,” *Website*: www. zte. com. cn

[2] Shahid Mumtaz, Jonathan Rodriguez, Linglong Dai, mmWave Massive MIMO. 2016

[3] Parchin, N. O. et al.: 'Eight-element dual-polarized MIMO slot antenna system for 5G smartphone applications', *IEEE Access*, 2019, 9, 15612–15622.

[4] Parchin, N. O. et al.: 'Mobile-phone antenna array with diamond-ring slot elements for 5G massive MIMO systems', *Electronics,* 2019, 8, 521

[5] Liu, D.; Hong, W.; Rappaport, T.S.; Luxey, C.; Hong, W, “What will 5G Antennas and Propagation Be? ”, *IEEE Trans. Antennas Propag*., 65, 6205–6212, 2017

[6] Hamza El Omari El Bakali, Alia Zakriti, Abdelkrim Farkhsi, Aziz Dkiouak and Mohssine El Ouahabi, “Design and Realization of Dual Band Notch UWB MIMO Antenna in 5G and Wi-Fi 6E by Using Hybrid Technique”, *Progress In Electromagnetics Research C*, Vol. 116, 1–12, 2021

[7] S. F. Jilani and A. Alomainy, “Millimetre-wave T-shaped MIMO antenna with defected ground structures for 5G cellular networks,” *IET Microwaves, Antennas Propag*., vol. 12, no. 5, pp. 672–677, 2018.

[8] A. K. Sohi and A. Kaur, “UWB aperture coupled circular fractal MIMO antenna with a complementary rectangular spiral defected ground structure (DGS) for 4G/WLAN/radar/satellite/international space station (ISS) communication systems,” *J. Electromagn. Waves Appl*., vol. 34, no. 17, pp. 2317–2338, 2020.

[9] N. N. Lan, “Gain enhancement in MIMO antennas using defected ground structure*,” Prog. Electromagn. Res*. M, vol. 87, no. September, pp. 127–136, 2019.

[10] N. O. Parchin, Y. Al-Yasir, A. Alabdullah, H. J. Basherlou, A. Abdulkhaleq, R. A. Abd-Alhameed and J. M. Noras, “8×8 MIMO antenna system with coupled-fed elements for 5G handsets,” *IET Conf. Publ*., vol. 2019, no. CP762, pp. 3–7, 2019.

[11] A. Gupta and V. Kumar, “DGS-based wideband MIMO antenna for on–off body communication with port isolation enhancement operating at 2.45 GHz industrial scientific and medical band,” *J. Electromagn. Waves Appl.*, vol. 35, no. 7, pp. 888–901, 2021.

[12] R. Sanmugasundaram, S. Natarajan, and R. Rajkumar, “A compact mimo antenna with electromagnetic bandgap structure for isolation enhancement,” *Prog. Electromagn. Res*. C, vol. 107, no. December 2020, pp. 233–244, 2021.

[13] N. K. Kiem and D. N. Chien, "A transmission line decoupling technique for enhancement of port isolation of dual-band MIMO antennas," *J. Electromagn. Waves Appl*., vol. 32, no. 10, pp. 1195–1211, 2018.

[14] C. Du, Z. Zhao, X. Wang, and F. Yang, "A compact cpw-fed triple-band mimo antenna with neutralization line decoupling for wlan/wimax/5g applications," *Prog. Electromagn. Res*. M, vol. 103, no. April, pp. 129–140, 2021.

[15] M. El Ouahabi, A. Zakriti, M. Essaaidi, A. Dkiouak, and H. Elftouh, "A miniaturized dual-band MIMO antenna with low mutual coupling for wireless applications," *Prog. Electromagn. Res*. C, vol. 93, no. May, pp. 93–101, 2019.

[16] G. Bharti, D. Kumar, A. K. Gautam, and A. Sharma, "Two-port dual-band circularly polarized dielectric resonator-based MIMO antenna with polarization diversity," *Electromagnetics*, vol. 40, no. 7, pp. 463–478, 2020.

[17] A. Dkiouak, A. Zakriti, and M. El Ouahabi, "Design of a compact dual-band MIMO antenna with high isolation for WLAN and X-band satellite by using orthogonal polarization," *J. Electromagn. Waves Appl.*, vol. 34, no. 9, pp. 1254–1267, 2019.

[18] A. Dkiouak, A. Zakriti, M. El Ouahabi, and A. Mchbal, "Design of two element Wi-MAX/WLAN MIMO antenna with improved isolation using a short stub-loaded resonator (SSLR)," *J. Electromagn. Waves Appl*., vol. 34, no. 9, pp. 1268–1282, 2020.

[19] A. Dkiouak, A. Zakriti, M. El Ouahabi, N. A. Touhami, and A. Mchbal, "Design of a four-element MIMO antenna with low mutual coupling in a small size for satellite applications," *Prog. Electromagn. Res*. M, vol. 85, no. July, pp. 95–104, 2019.

[20] Y. A. S. Dama, R. A. Abd-Alhameed, S. M. R. Jones, D. Zhou, N. J.McEwan,M. B. Child, and P. S. Excell, "An Envelope Correlation Formula for (N,N) MIMO Antenna Arrays Using Input Scattering Parameters, andIncluding Power Losses",International Journal of Antennas and Propagation, August 2011.

[21] Chae S, Oh S,Park S. Analysis of mutual coupling, correlations, and TARC in MIMO antenna array. 2(6):2–5.

[22] E. Fritz-Andrade, H. Jardon-Aguilar, and J. A. Tirado-Mendez, "The correct application of total active reflection coefficient to evaluate MIMO antenna systems and its generalization to N ports," *Int. J. RF Microw. Comput. Eng*., vol. 30, no. 4, pp. 1–10, 2020.

[23] M. S. Sharawi, "Printed multi-band MIMO antenna systems and their performance metrics," *IEEE Antennas Propag. Mag*., vol. 55, no. 5, pp. 218–232, 2013.

[24] A. H. Jabire et al., "Metamaterial based design of compact UWB/MIMO monopoles antenna with characteristic mode analysis," *Appl. Sci*., vol. 11, no. 4, pp. 1–21, 2021.

[25] K. S. Sultan and H. H. Abdullah, "Planar UWB MIMO-Diversity Antenna with Dual Notch Characteristicst," *Prog. Electromagn. Res. C*, vol. 93, no. May, pp. 119–129, 2019.

[26] Valderas, D., Crespo, P., & Ling, C. , "UWB portable printed monopole array design for MIMO communications," *Microwave and Optical Technology Letters*, 52(4), 889–895, 2010.

[27] G. J. Foschini, "Layered space-time architecture for wireless communication in a fading environment when using multi-element antennas," *Bell Labs Tech*. J., vol. 1, no. 2, pp. 41–59, 1996.

[28] E. TELATAR, "Capacity of Multi-antenna Gaussian Channels," *Eur. Trans. Commun*., vol. 10, no. 6, pp. 585–595, 1999.

[29] M. A. Jamshed, M. Ur-Rehman, J. Frnda , A. A. Althuwayb, A. Nauman and K. Cengiz, "Dual Band and Dual Diversity Four-Element MIMO Dipole for 5G Handsets," *Sensors*, 21(3), 767, 2021.

[30] A. Khurshid, J. Dong, M. S. Ahmad, and R. Shi, "Optimized Super-Wideband MIMO Antenna with High Isolation for IoT Applications," *Micromachines*, vol. 13, no. 4, 2022.

[31] V. Rajeshkumar and R. Rajkumar, "SRR loaded compact tri-band mimo antenna for wlan/wimax applications," *Prog. Electromagn. Res. Lett.*, vol. 95, no. January, pp. 43–53, 2020.

[32] J. A. Tirado-Méndez, H. Jardón-Aguilar, A. Rangel-Merino, L. A. Vasquez-Toledo, and R. Gómez-Villanueva, "Four ports wideband drop-shaped slot antenna for MIMO applications," *J. Electromagn. Waves Appl.*, vol. 34, no. 9, pp. 1159–1179, 2020.